2013

Structural and thermodynamic dissection of linear motif recognition by the E. coli sliding clamp

Zhou Yin
University of Wollongong, zy877@uowmail.edu.au

Michael J. Kelso
University of Wollongong, mkelso@uow.edu.au

Jennifer L. Beck
University of Wollongong, jbeck@uow.edu.au

Aaron J. Oakley
University of Wollongong, aarono@uow.edu.au

Publication Details

Yin, Z., Kelso, M. J., Beck, J. L. & Oakley, A. J. (2013). Structural and thermodynamic dissection of linear motif recognition by the E. coli sliding clamp. Journal of Medicinal Chemistry, 56 (21), 8665-8673.

Structural and thermodynamic dissection of linear motif recognition by the E. coli sliding clamp

Abstract
Protein-protein interactions based on linear motif (LM) recognition play roles in many cell regulatory processes. The E. coli sliding clamp is a protein mediator of replisome formation, which uses a common surface pocket composed of two subsites (I and II) to interact with LMs in multiple binding partners. A structural and thermodynamic dissection of sliding clamp-LM recognition has been performed, providing support for a sequential binding model. According to the model, a hydrophobic C-terminal LM dipeptide submotif acts as an anchor to establish initial contacts within subsite I, and this is followed by formation of a stabilizing hydrogen-bonding network between the flanking LM residues and subsite II. Differential solvation/desolvation during positioning of the submotifs is proposed as a driver for the sequential binding. Our model provides general insights into linear motif recognition and should guide the design of small-molecule inhibitors of the E. coli sliding clamp, an emerging antibacterial target.

Keywords
structural, thermodynamic, recognition, coli, dissection, linear, e, motif, clamp, sliding, CMMB

Publication Details
Yin, Z., Kelso, M. J., Beck, J. L. & Oakley, A. J. (2013). Structural and thermodynamic dissection of linear motif recognition by the E. coli sliding clamp. Journal of Medicinal Chemistry, 56 (21), 8665-8673.

Structural and Thermodynamic Dissection of Linear Motif Recognition by the *E. coli* Sliding Clamp

Zhou Yin,[†] *Michael J. Kelso,*[†] *Jennifer L. Beck*[†] *and Aaron J. Oakley* [*, †]

[†] School of Chemistry, University of Wollongong, Northfields Ave, Wollongong 2522, NSW, Australia

ABSTRACT: Protein-protein interactions based on linear motif (LM) recognition play roles in many cell regulatory processes. The *E. coli* sliding clamp is a protein mediator of replisome formation, which uses a common surface pocket composed of two sub-sites (I and II) to interact with LMs in multiple binding partners. A structural and thermodynamic dissection of sliding clamp-LM recognition has been performed, providing support for a sequential binding model. According to the model a hydrophobic C-terminal LM dipeptide sub-motif acts as an anchor to establish initial contacts within subsite I and this is followed by formation of a stabilizing hydrogen-bonding network between the flanking LM residues and subsite II. Differential solvation/desolvation during positioning of the sub-motifs is proposed as a driver for the sequential binding. Our model provides general insights into linear motif recognition and should guide the design of small-molecule inhibitors of the *E. coli* sliding clamp, an emerging antibacterial target.

INTRODUCTION

Protein-protein interaction sites govern numerous biological processes and are a well-known class of drug targets.[1] Linear motifs (LMs) are short (4-10 residues) intrinsically disordered sequences that are often found at the termini of proteins and sometimes in loop regions.[2-4] Recognition of LMs[5, 6] by rigid protein domains represents a distinct category of protein-protein interaction, with many examples involved in cell signaling, DNA replication and other cell-regulatory processes.[7-9] Recognition of LMs by their partner proteins often shows both specific and promiscuous characteristics.[10] Promiscuity arises because the protein acts as a binding "hub" capable of interacting with multiple partners bearing distinct (but related) LMs.[10, 11] Specificity arises from the interaction of conserved LM "anchor" residues[12-14] with target receptor "hot spots",[15, 16] which when removed lead to loss of binding affinity. In general, LM recognition events are transient and show only weak affinity (1–100 μM)[17] and it has been proposed that this may arise from the configurational entropy loss that occurs when LMs adopt the bound conformation.[18] This is supported by the fact that most LM peptides do not induce conformational changes in their binding partners.[16] Hydrophobic residues commonly found in LMs are also thought to contribute entropically favorable desolvation free energy to the binding.[3, 19, 20] A sequential model of LM-binding via partially bound states has been proposed and is consistent with the typically observed fast on-and-off binding kinetics.[12, 13, 21]

While there is growing interest in the design of drugs targeting LM-recognition sites[22, 23] these efforts are being hampered by a lack of further mechanistic insights into the binding process. Additional structural evidence in support of the sequential binding model is required along with further evidence connecting LM characteristics with their dynamic behavior.

The *E. coli* sliding clamp (SC), also known as the DNA polymerase III *β* subunit and the *β*-clamp, is a protein-protein interaction hub that plays a central role in the bacterial DNA replication and repair

machinery. It is distinctly different from and shares only topological similarity with its eukaryotic counterpart, the proliferating cell nuclear antigen (PCNA).[24, 25] The SC is a torus-shaped dimer that surrounds double-stranded DNA functioning to recruit various binding partners to DNA.[25] A single binding pocket on each clamp monomer interacts with LMs in the various partners.[26-28] The diverse range of proteins that interact with the SC makes it one of the most trafficked elements in the cell protein network.[28] Interacting proteins include the δ-clamp loading subunit of DNA Pol III, DNA pol I, II, IV, VI and MutS.[29, 30] The central role played by the SC in multiple essential functions in bacteria and its structural divergence from PCNA make it an attractive antibacterial target.

The LMs of SC binding partners are usually found at their N/C-termini and these isolated peptides tend to bind to the SC with affinities similar to their parent proteins.[31, 32] Conversely, when LMs are removed the truncated proteins lose all binding affinity.[33] Previous studies have shown that the consensus motif (QLx_1Lx_2F/L: S/D preferred at x_1, x_2 may be absent) binds to a specific pocket on the SC monomer comprised of two subsites, I and II.[34, 35] A pentapeptide derived from the consensus motif, $Ac_0Q_1L_2D_3L_4F_5$ (subscripts denoting position), binds to the SC with equivalent affinity to SC-binding proteins ($K_d \sim 1$ μM) and is considered the minimal binding motif.[31, 36]

In the current study, a combination of biochemical/biophysical assays and structural and theoretical approaches have been used to unravel key mechanistic insights into *E. coli* SC-LM recognition. Single-residue substitutions of the $Ac_0Q_1L_2D_3L_4F_5$ consensus peptide were used to characterize the binding determinants and to elucidate the structural basis for the specificity of LM-binding. The weak and transient nature typical of LM recognition was computationally probed with supporting evidence provided from calorimetric data. The study has led us to propose a sequential binding model wherein the anchor residues of the LM establishes initial contacts with subsite I, followed by binding of the flanking residues to subsite II. The model is supported by steered molecular dynamics (SMD) simulations and crystal structures, which provide snapshots into the sequential binding pathway. The

desolvation/resolvation profile of almost-buried polar atoms (ABPA)[37] is shown to account for the priority of anchor-residue positioning over positioning of other residues in the LM.

RESULTS AND DISCUSSION

Interactions of Q_1 with subsite II and L_4F_5 with subsite I. The published X-ray crystal structure of the consensus pentapeptide $Ac_0Q_1L_2D_3L_4F_5$ in complex with the *E. coli* SC (PDB entry3Q4J)[36] is shown in Figure 1A. In this structure the N-terminal $Ac_0Q_1L_2$ dipeptide sub-motif occupies subsite II making three H-bonds to the backbone amides of M362, P363 and R365, and one H-bond to a bridging water molecule (W_0). The side-chain of L_2 is involved in hydrophobic interactions with P363. The non-polar C-terminal L_4F_5 dipeptide sub-motif occupies subsite I and makes interactions with the hydrophobic side-chains of L177, V247, V360 and M362. In the current work, X-ray crystal structures of the SC were obtained in complex with all five possible alanine mutants of the consensus peptide; $AcA_1L_2D_3L_4F_5$, $AcQ_1A_2D_3L_4F_5$, $AcQ_1L_2A_3L_4F_5$, $AcQ_1L_2D_3A_4F_5$ and $AcQ_1L_2D_3L_4A_5$ (Complexes are denoted $SC^{AcALDLF}$, $SC^{AcQADLF}$, $SC^{AcQLALF}$, $SC^{AcQLDAF}$ and $SC^{AcQLDLA}$; Figure 1B–F. Crystallographic data are provided in Table S1). The individual structures are discussed below in the context of their SC binding affinities.

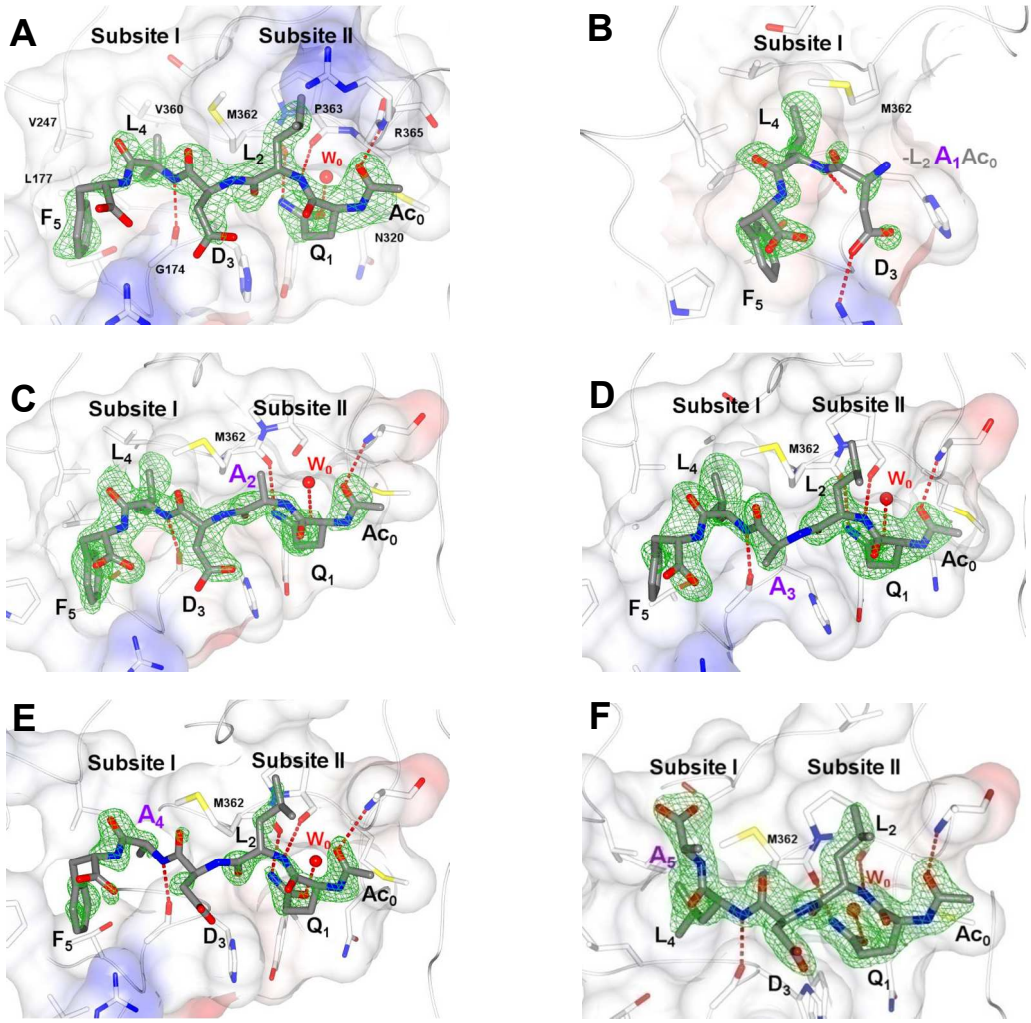

Figure 1. Crystal structures of the *E. coli* SC bound to$Ac_0Q_1L_2D_3L_4F_5$ consensus peptide ($SC^{AcQLDLF}$, **A**)[36]and its alanine mutants: $SC^{AcALDLF}$ (**B**), $SC^{AcQADLF}$ (**C**), $SC^{AcQLALF}$ (**D**), $SC^{AcQLDAF}$(**E**) and $SC^{AcQLDLA}$ (**F**).The complexes are shown with the SC carbon atoms shaded white and with the peptide carbon atoms colored grey (all other atoms in CPK colors). Electrostatic potential surfaces of the binding-site are shown with blue = positive and red = negative. Dashed lines in red represent H-bonds. A bridging water molecule (W_0) is shown as a red sphere. Electron density maps (mF_o–DF_c) contoured at 3σ are shown in green wire-basket form.

The binding contribution of each residue in $Ac_0Q_1L_2D_3L_4F_5$ was probed using a series of mutant peptides (Table 1). Alanine mutants were used to assess relative side chain contributions, and glycine mutants were used to show the impact of backbone flexibility on affinity by way of comparison with the alanine mutants. Other mutations were to residues with similar polarity, functional groups and/or shape so as to differentiate the importance of each of these aspects to peptide binding. Binding affinities for the mutants were measured using a fluorescence polarization (FP) assay employing a fluorescently labeled tracer peptide (K_d = 70 nM, determined with binding-saturation curve fitting). Inhibition of tracer binding to the SC was plotted against peptide concentrations and their IC_{50} values calculated and transformed into K_d using the Kenakin correction for ligand depletion (Table 1).[38]

Table 1. Effects of single-residue mutations on LM consensus peptide binding to the SC.

Mutation	Peptide	IC_{50}(μM)	K_d (μM)	ΔG (298K) (kcal/mol)	[a]ΔΔG	[b]$\Delta\Delta\Delta G_{A-G}$
	AcQLDLF	1.9	0.9	–8.3	0.00	
Ac_0	QLDLF	63.2	29.5	–6.2	2.10	
Q_1	AcELDLF	222.1	103.6	–5.5	2.85	
	AcNLDLF	43.6	20.3	–6.4	1.88	
	AcALDLF	602.6	281.2	–4.9	3.44	
	AcGLDLF	976.5	455.7	–4.6	3.73	0.29
L_2	AcQVDLF	60.4	28.2	–6.2	2.07	
	AcQADLF	78.6	36.7	–6.1	2.23	
	AcQGDLF	36.1	16.8	–6.5	1.76	-0.46
D_3	AcQLALF	3.4	1.6	–7.9	0.37	
	AcQLGLF	10.4	4.9	–7.3	1.03	0.66
L_4	AcQLDVF	1215.0	567.0	–4.4	3.86	
	AcQLDAF	246.7	115.1	–5.4	2.91	
	AcQLDGF	1524.0	711.2	–4.3	3.99	1.08
F_5	AcQLDLL	20.96	9.8	–6.9	1.44	
	AcQLDLA	555.2	259.1	–4.9	3.39	
	AcQLDLG	1067.0	497.9	–4.5	3.78	0.39

[a] Binding energy difference compared to AcQLDLF. [b] Difference in binding energy upon replacing alanine with glycine.

The acetylated N-terminus (Ac_0) of AcQLDLF mimics the main-chain of LMs by providing a carbonyl oxygen to accept a H-bond (Figure 1A). Replacing Ac_0 with a charged primary amine at the N-terminus significantly decreased affinity (Table 1). Replacing Q_1 with glutamate increased K_d significantly but substitution with asparagine, which has a shorter side chain, led only to a modest increase. Reducing Q_1 down to alanine or glycine greatly reduced affinity and this change also precluded correct positioning of the $Ac_0A_1L_2$ sub-motif, as evidenced by the lack of electron density in the map of the $SC^{AcALDLF}$ complex (Figure 1B). These findings establish the crucial importance of the two H-bonds formed from the Q_1 side-chain for binding in subsite II.

Replacing the hydrophobic residue L_2 with valine, alanine or glycine had less effect on binding than changes at Q_1, while substituting D_3 for alanine or glycine had almost no effect. Additionally, replacing L_2 or D_3 with alanine did not alter the bound peptide conformations (Figure 1C and1D relative to 1A).

Substitution of L_4 with valine had a strongly detrimental effect on binding, highlighting the strict steric requirements for binding in this region of subsite 1. Replacing L_4 with alanine significantly reduced affinity as well as crystallographic ligand occupancy, as evidenced by the poor peptide electron density in the $SC^{AcQLDAF}$ complex (Figure 1E). A glycine residue at this position further reduced affinity. The significant difference in binding energy observed for the alanine-*versus*-glycine substituted peptides at position 4 ($\Delta\Delta\Delta G$ = 1.08 kcal/mol; Table 1) may be due to the higher flexibility of glycine. This increased flexibility would impose a larger entropic cost upon binding and reduce the likelihood of G_4F_5 binding in subsite I and triggering subsequent subsite II binding events (see sequential binding model below).

Replacement of F_5 with leucine produced a modest increase in K_d but, in cases with alanine or glycine, there was detrimental effect on binding that was similar to the same substitutions at the L_4 position. Interestingly, the $SC^{AcQLDLA}$ complex structure (Figure 1F) showed that replacement of F_5

with alanine causes this residue to be flipped out of subsite I leaving half of the subsite unoccupied. This is consistent with a sub-motif (e.g. L_4F_5) needing to fully occupy subsite I before binding interactions are triggered in subsite II (see sequential binding model below).

Entropy loss upon binding diminishes linear motif affinity for the *E. coli* SC. The alanine and glycine scans above showed that these mutations significantly reduce binding affinity, with a higher penalty observed for glycine (except at position L_2). This can be explained by the reduced hydrophobic interactions possible with glycine (*vs.* alanine) and because of the higher flexibility of glycine residues. Since glycine can adopt a greater range of backbone phi/psi angles compared to alanine there is a greater entropic cost associated with glycine-containing peptides.

Molecular dynamics (MD) simulations and molecular mechanics (MM) calculations with Poisson-Boltzmann Surface Area (PBSA) solvation were performed to decompose the energy of LM peptides binding to the SC and to quantify the contribution of ligand deformation entropy. The following equation shows how the changes in Gibbs free energy (ΔG) were decomposed:[39]

$$\Delta G = G_{complex} - G_{receptor} - G_{ligand}$$

$$= E_{MM} + E_{solv} + E_{def} - T\Delta S$$

$$= E_{vdw} + E_{elec} + E_{pb} + E_{cavity} + E_{def} - T\Delta S$$

Briefly, E_{MM} represents the molecular mechanics (MM) interaction energy difference upon complex formation, comprised of the van der Waals (VDW) interaction energy (E_{vdw}) and electrostatic interaction energy (E_{elec}). E_{solv} is the difference in solvation energy and is comprised of E_{pb} and E_{cavity}. Both E_{MM} and E_{solv} were calculated for the complex using a single-trajectory approach.[39] The ligand energy difference upon binding (deformation energy, E_{def}) was calculated from a separate MD simulation and MM/PBSA calculation on the free peptide alone (E_{Free}), and the energy of the bound

peptide (E_{bound}). Receptor deformation in the calculation of E_{MM} and E_{solv} was ignored. Conformational entropy ($-T\Delta S$) was calculated using the triple-trajectory approach with normal mode analysis.[39]

Table 2. MD simulation and MM-PBSA calculation data for peptides binding to the *E. coli* SC (units in kcal/mol, details in Table S2).

	$E_{MM} + E_{solv}$	E_{def}	$-T\Delta S_{def}$	$-T\Delta S$	ΔG
AcQLDLF	–49.6	1.4	6.5	20.8	–27.3
AcALDLF	–40.7	3.2	4.2	21.6	–15.8
AcQADLF	–45.9	–0.1	5.5	18.3	–27.7
AcQLALF	–47.3	–0.8	–1.1	22.5	–25.6
AcQLDAF	–44.4	0.4	4.8	20.2	–23.8
AcQLDLA	–45.7	2.0	4.2	23.6	–20.1

Although the calculations did not reproduce the experimentally determined binding free energies (Table 2),[36] they performed well in distinguishing the good from the poor binders amongst similar peptides and in a pattern consistent with the FP data (Table 1). Ligand deformation energy (E_{def}) was similar among the peptides relative to AcQLDLF. Ligand deformation entropy ($-T\Delta S_{def}$) represents the difference between the conformation entropy of bound and free peptide. In almost all cases, the entropic cost of ligand deformation ($-T\Delta S_{def}$) accounts for a significant portion of the unfavorable conformational entropy loss ($-T\Delta S$) and thus the Gibbs energy (ΔG).

Isothermal titration calorimetry (ITC) was used to provide corroborative evidence of ligand deformation on entropy. Entropy differences ($-T\Delta S$) derived from the ITC measurements represent global values, hence not identical to the corresponding term in the computational studies (Table 2). Only strongly binding peptides were examined in these experiments as ligand solubility and receptor

concentration placed limitations on the measurable binding constants. The ΔG values from the ITC measurements (Table 3) were found to be consistent with the FP results (Table 1).

Table 3. Thermodynamic data for peptides binding to the *E. coli* SC as determined by ITC (at 298K, units in kcal/mol).

		ΔH	**–TΔS**	**ΔG**
	AcQLDLF	–13.66	5.36	–8.30
Ac_0	QLDLF	–6.39	0.35	–6.03
Q_1	AcNLDLF	–7.40	1.83	–5.57
L_2	AcQVDLF	–11.93	5.60	–6.33
	AcQADLF	–13.60	7.21	–6.39
	AcQGDLF	–14.66	8.05	–6.61
D_3	AcQLALF	–12.18	3.73	–8.46
F_5	AcQLDLL	–11.00	3.99	–7.01

The greatly reduced entropic cost of binding observed when Q_1 was mutated to asparagine suggests that the bound N_1-containing peptide is poorly ordered. This correlates well with the poorly ordered peptide structure observed in the $SC^{AcALDLF}$ crystal structure (Figure 1B). The peptide lacking the Ac_0 group is probably also disordered when bound given its low binding entropic penalty. The entropic costs of binding for peptides with mutations at positions L_2, D_3 and F_5 were all similar to the reference peptide, suggesting these would likely adopt similar peptide-binding poses to that observed in the reference $SC^{AcQLDLF}$ structure. In the cases of D_3 and F_5 replacement, it is likely that reductions in residue size and the resulting reductions in desolvation energy produced the net reductions in entropic

cost of binding when compared to the reference AcQLDLF peptide.

Replacement of L_2 with valine, alanine or glycine showed similar binding enthalpy with increased entropic costs of binding compared with the reference peptide. This may be explained by the higher flexibility (and hence conformational entropy) of unbound peptides containing smaller side chains at position 2 resulting in increased entropy loss upon binding of these peptides to the SC. This supports our hypothesis that differences in ligand deformation accounts for a significant part of the entropy of binding. By comparison, F_5 is a terminal residue and its contribution to overall vibrational freedom (and hence conformational entropy) would be smaller.

An anchor-based sequential binding model for LM recognition by the *E. coli* SC. The impact of A or G mutations at L_4 on binding affinity, as measured by FP (Table 1), suggested a crucial role for this residue in the binding process: the alanine mutant had reduced affinity due to reduced interaction, while the glycine mutant impaired binding to a much greater extent. We propose that deformation entropy of the ligand cannot fully account for the disproportionate effect of alanine to glycine substitution at position L_4 (and to a lesser extent D_3) compared to other positions. This finding led us to propose a sequential binding model whereby the L_4F_5 sub-motif establishes primary contacts with the subsite I pocket, which is then followed by orientation and binding of the flanking residues of the peptide in subsite II. According to this model, the entropic penalty of ligand deformation for glycine mutations at the D_3 or L_4 positions would disfavor subsequent binding of the $Ac_0Q_1L_2$ sub-motif. This model can explain the impact of mutations on the kinetic constants of LM association and dissociation, with surface plasmon resonance experiments having shown that such interactions are fast-on and fast-off,[32] a feature that is commonly observed in LM binding.[40] Given the rapid kinetics, we reasoned that the dissociation phenomenon was amenable to steered molecular dynamics (SMD) simulations.

The early dissociation process of the $Ac_0Q_1L_2A_3L_4F_5$ mutant peptide from the SC was chosen for the

simulation. The D_3 to alanine mutant was used because of its small size and because D_3 was shown to make only a minor contribution to the binding energy. Three calculations were performed where steering forces were applied to the mass centers of (1) the whole peptide, (2) the $Ac_0Q_1L_2$ and (3) L_4F_5 sub-motifs (Figure 2). The Boltzmann-averaged cumulative work calculated after Jacobian correction[41] suggested that the L_4F_5 sub-motif is more likely to dissociate from the complex first as it requires the least work (i.e. shallowest slope in the trajectory). Additionally, the calculations showed that a lower energy barrier lies along the L_4F_5 binding/dissociating pathway in comparison with the pathway in which $Ac_0Q_1L_2$ dissociates first (as indicated by reduced cumulative work).

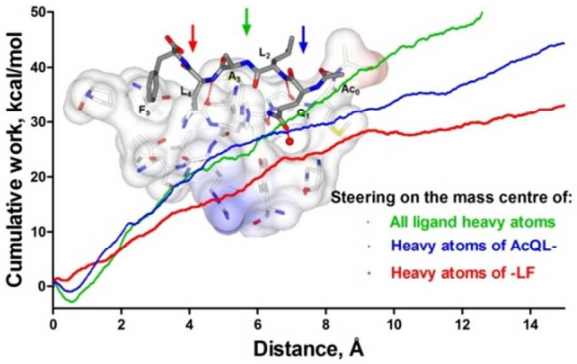

Figure 2. Plot of cumulative work *vs.* distance during SMD simulated dissociation of AcQLALF from the SC. Steering forces were applied to the three different centers of mass indicated.

Binding of the dipeptides AcQL, AcLF (and their various C/N-terminal variants) to the SC was next assessed by FP assay and X-ray crystallography to test the hypothesis that the L_4F_5 sub-motif must bind/unbind first. AcQL and its analogues failed to show any binding to the clamp by either method (Table S3). In contrast, AcLF and its analogue 4MF ((*S*)-2-(4-methylpentanamido)-3-phenylpropanoic acid) showed weak affinity (IC_{50}=1.1 and 4.44 mM respectively, Table S3) and both were shown to occupy subsite I in their respective X-ray structures, SC^{AcLF} and SC^{4MF} (Figure 3A–C, crystallographic data in Table S4). AcQL and its C-terminal variants failed to demonstrate binding by X-ray crystallography even when AcLF was pre-bound into subsite I (crystallographic data not shown).

The SC^{4MF} complex structure, determined in space group (P1), showed that binding of 4MF causes a minor perturbation of the binding pocket at S346 and H175 (Figure 3A) when compared with an apo-SC structure determined in the same space group (SC^{P1}, crystallographic data in Table S4). A gating residue M362 retains a "closed" conformation (Chi_2 angle –177°) in both of these structures, which blocks the passageway between subsites I and II (Figure 3A).

The structure of the SC^{AcLF} complex, determined in space group $P2_1$, showed that binding of dipeptide AcLF to chain B of the SC (Figure 3B) causes no apparent changes in the binding site, as compared with the apo-clamp structure determined in the same space group (PDB entry 1MMI, Figure 3B). In both of these structures, the M362 gating residue retains the “closed” conformation. However, when the same dipeptide bound to chain A (Figure 3C) the binding features observed were similar to those seen with longer peptides (e.g. AcQLDLF and DNA Pol IV little finger domain, Figure 3D), including movements in the side-chains of M362 and S364. The binding observed in chain B appears to be due to stabilization by a nearby symmetry-related molecule (Figure S2) and may represent a pre-equilibrium state, with equilibrium binding guided by desolvation and formation of a H-bond between the L_4 amide and G174 carbonyl groups. The gating residue M362 is unmoved in chain B (Chi_2 angle –170°) but is in a "half-open" conformation (Chi_2 angle –74° and -93° for alternate conformers) in chain A, exposing the G174 carbonyl group as a H-bond acceptor.

The SC^{AcLF} and SC^{4MF} crystal structures suggest that the L_4F_5 sub-motif acts as an anchor capable of binding on its own. We propose that the SC^{4MF}, SC^{AcLF} and $SC^{AcQLALF}$ complex structures exemplify snapshots along the pathway to binding. The compound 4MF bound in subsite I highlights the initial contact, while AcLF makes an additional H-bond with G174 and subsequently triggers partial opening of the M362 gate. AcQLALF occupies subsite I and subsite II with the M362 in the fully "open" conformation (Chi_2 55°, Figure 3D). The SMD simulation of AcQLALF dissociation (Figure 2) demonstrated that “pulling” the anchor sub-motif (L_4F_5) reduces the energetic barrier for dissociation

of the rest of the peptide.

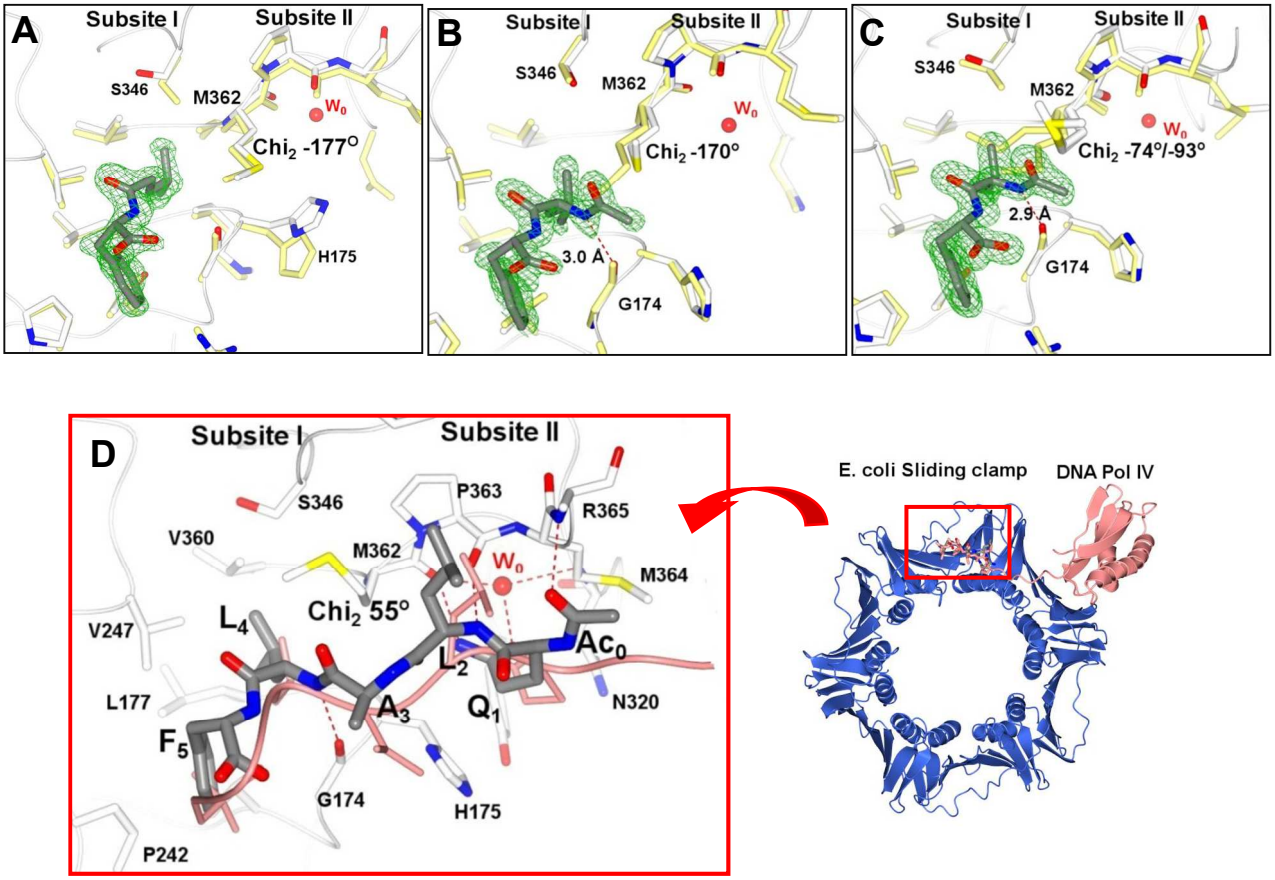

Figure 3. Crystal structures of SC^{4MF} (**A**), and SC^{AcLF} chain B (**B**) and SC^{AcLF} chain A (**C**). SC residues are presented in white with non-carbon atoms CPK colored. Structures of the equivalent native SC structures with equivalent crystal packing are superimposed and shown in yellow (SC^{P1} onto SC^{4MF}, 1MMI chain B and A onto SC^{AcLF} chain B and A, respectively). The peptide atoms are CPK colored. Dashed lines in red represent H-bonds. Electron density maps (mF_o–DF_c) contoured at 3σ are shown in green wire-basket form. (**D**) The crystal structure of the SC/Pol IV little finger domain (PDB entry 1UNN) is shown superimposed onto $SC^{AcQLALF}$. The DNA Pol IV little finger domain is shown in pink. The enlarged view of the binding pocket in the $SC^{AcQLALF}$ structure shows the SC pocket (white), the AcQLALF peptide (grey). Non-carbon atoms are CPK colored. Dashed lines in red represent H-bonds. A bridging water molecule (W_0) is shown as a red sphere.

In summary, the model proposes that the binding (or unbinding) of the L_4F_5 anchor sub-motif triggers subsequent binding (or unbinding) of the $Ac_0Q_1L_2$ sub-motif. Acting together, these two sub-motifs contribute most of the binding energy of the consensus motif, as evidenced by the FP data. Since the binding of the consensus motif to the SC determines the binding of the entire protein,[31, 33] the binding of the consensus motif should precede the binding of the rest of protein. For instance, in the case of the "little finger" domain of DNA Pol IV (PDB entry 1UUN, Figure 3D), the terminal residues equivalent to the consensus motif should initiate both binding and unbinding.

Almost-buried polar atoms (ABPAs) present a kinetic barrier. The mutational analysis of consensus peptide binding suggested equal importance for the L_4F_5 and Ac_0Q_1 motifs to affinity, with the L_4F_5 sub-motif functioning as an anchor to initiate binding. Initially we thought that the "closed" conformation of M362 was acting as a gate blocking binding at subsite II. However, MD simulations of the native SC monomer showed that the M362 Chi_2 angles corresponding to the open/closed conformations are equally populated in the trajectory (Figure S3), suggesting that the conformation of M362 is probably not determining the order of binding.

We instead propose that a kinetic barrier, caused by differences in the nature of desolvation and resolvation of subsites I and II, is responsible for L_4F_5 acting as the anchor sub-motif. Subsite I consists mostly of hydrophobic residues that contact the side-chains of L_4F_5 (Figure 4A). In contrast, subsite II makes multiple H-bonds with the $Ac_0Q_1L_2$ sub-motif (Figure 4B), including some mediated by the bridging water (W_0). The trajectory of a 5 ns native SC simulation, which included all crystallographic water molecules, showed that W_0 remained bound (Figure S4) and was tightly restrained by H-bonds to M362O and N320N (Figure S5). It was therefore concluded that $W_0$is a structural water molecule in the SC.

A recent study showed that H-bond interactions between the protein and ligands that are shielded

from bulk solvent contribute to slow binding/unbinding kinetics.[37] This was explained by the desolvation and resolvation of "almost-buried polar atoms" (ABPAs) upon ligand binding/unbinding, which involves a transition state that is energetically unfavorable because it occurs asynchronously with dehydration/rehydration.[37] ABPA refers to atoms with < 10 $Å^2$ solvent accessible surface area (SASA) located within a concave site where the ΔSASA is < 0 (change of SASA with increased probe radius). For the *E. coli* SC, W_0 and M362O are ABPA atoms according to this definition while all other polar atoms making H-bonds in both subsites I and II are non-ABPAs (Table S5).

To determine the role of W_0 and M362O as ABPAs along the proposed dissociation pathway, we performed SMD simulations of a model AcQL dipeptide dissociating from subsite II, using initial coordinates from the $SC^{AcQLALF}$ complex structure. For comparison, a SMD simulation was carried out for dissociation of AcLF from subsite I, using coordinates from the SC^{AcLF} complex as the starting structure. The AcLF dipeptide makes one H-bond with a G174O, a non-ABPA. Jacobian corrections were applied in the cumulative work calculations.[41]

The cumulative work plot for AcLF dissociation is uniformly ascending showing only one energetic minimum (Figure 4C). As a non-ABAP, the G174O in subsite I is solvent accessible even when AcLF is bound (Figure 4G). The breaking of the H-bond with the dissociating AcLF (Figure 4E) is offset by increasing contacts with bulk solvent (Figure 4G), thus no kinetic barrier is observed in the case of AcLF dissociation (Figure 4C).

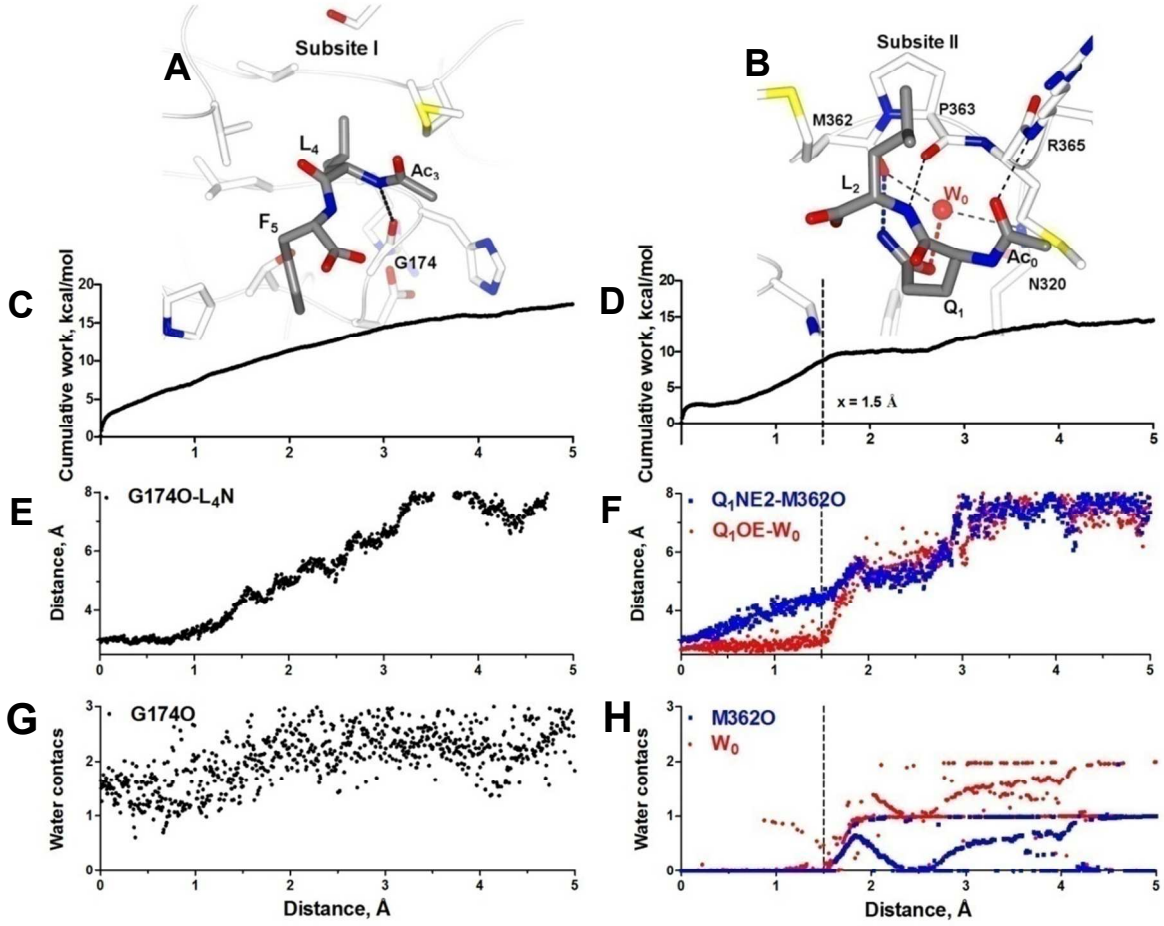

Figure 4. (**A**, **B**) Model structures for SMD simulation of AcLF and AcQL dissociation from subsites I and II, respectively. The dipeptides are colored grey and the binding pockets white. Non-carbon atoms are CPK colored. Dashed lines represent H-bonds. A bridging water (W_0) is shown as a red sphere. (**C**, **D**) Boltzmann averaged cumulative work of the dipeptides pulled for 5 Å from the mass center of the pockets. (**E**, **F**) Distances of H-bond pair atoms presented as a Boltzmann average of 20 simulation trajectories. (**G**, **H**) Number of water contacts (<3.4 Å) Boltzmann averaged with 20 simulation trajectories.

The cumulative work of steered dissociation of the model AcQL began with a steep ascending curve that quickly flattened (Figure 4D). This represents the peak of an energy barrier where the system could dissociate or re-associate. Dissociation was accompanied by the breakage of the H-bond between the W_0 and the Q_1 side-chain (Figure 4F) and reformation of H-bonds with the solvent (i.e. first layer resolvation) (Figure 4H). Breakage of the H-bond between M362O and the Q_1 side-chain preceded breakage of the W_0 to Q_1 H-bond (Figure 4F), while resolvation of M362O was insignificant (Figure 4H). At a distance of 1.5 Å, abrupt dissociation of the W_0 to Q_1 H-bond occurs, leading to greater movement of the Q_1 side-chain (Figure 4F) and formation of the first solvent layer in subsite II. Prior to this event, W_0 is completely shielded from bulk solvent. Thus, there was a transient state (distance <1.5 Å) where the system increases in energy as the H-bond with W_0 is broken with no compensatory formation of H-bonds with the first solvation layer.

We propose that the desolvation and resolvation of the structural water W_0 as an ABPA represents the kinetic barrier on the pathway of ligand dissociation and association and thus have an impact on the ligand affinity. Conversely, binding of AcLF to the SC is not opposed by this barrier as it is not present in subsite I. A similar kinetic barrier was observed in the work plot for the SMD simulation of the $SC^{AcQLALF}$ complex structure steered at the $Ac_0Q_1L_2$ sub-motif (Figure 2).

CONCLUSION

This study has identified two critical subsite-specific interactions: (1) the non-polar contacts of the L_4F_5 sub-motif with subsite I, and (2) the H-bond network of the Q_1 residue with subsite II mediated by a structurally conserved water molecule. We propose that the L_4F_5 sub-motif establishes primary contact with subsite I and that binding is entropically favorable due to

desolvation of the hydrophobic L_4F_5 sub-motif and binding site. Anchoring of the L_4F_5 sub-motif assists the Q_1 side-chain in overcoming the kinetic barrier caused by formation of H-bonds with the conserved water as an ABPA of subsite II. The H-bond network formed upon positioning of Q_1 in subsite II stabilizes the complex as the kinetic barrier similarly opposes association and dissociation. Dissociation occurs in the same order with the L_4F_5 sub-motif dissociating first.

This sequential binding model for ligand recognition by the *E. coli* SC could inform design strategies for small-molecule inhibitors as probes or drugs, if the critical interactions are to be reproduced.

To date, inhibition of LM recognition for therapeutic purposes has yielded few successes. Despite the similarities, LM recognition may differ in the composition of the anchor motif (e.g. phosphoserine/threonine-containing anchor motif recognized by SH2/WW domains,[42] PxxP binding to SH3 domain[43]) and potential structural transformation (folding-coupled binding in the case of P53 binding to MDM2[44]). These factors complicate any effort to completely elucidate the binding process. The LM recognition by the *E. coli* SC is a relatively simple case where the binding has no allosteric consequences, allowing the effect of the sub-motifs to be partitioned. The sequential binding model with differential solvation as a key driver revealed here may also apply to evolutionarily related and/or biochemically similar systems, such as the PCNA-mediated interactions in eukaryotic DNA replication *via* recognition of a -Qxx[I/L]xxFF motif.[24] Taking into account those structural and kinetic factors will assist drug design efforts targeting these systems.

Materials and Methods

Protein over-expression, purification and crystallization. The protein production and purification followed the published protocol.[45] Crystals were grown at 285 K by the hanging-

drop vapor diffusion method. The hanging drop was composed of 1 µl of SC (53 mg/ml) mixed with the same volume of a reservoir solution composed of 100 mM MES pH 6.5, 100-150 mM $CaCl_2$ and 25-30%(v/v) PEG400.The reservoir volume was 1 ml. Ligands were soaked into the crystal at 2-5 mM with <10 % DMSO.

X-ray data collection. All crystals were mounted onto MiTeGen™ loops on pins with magnetic caps. For in-house data collection, crystals were flash-frozen to 100 K using an Oxford Cryo-stream. Diffraction data were collected using a MAR345 desktop beamline using CuKα X-ray from a Rigaku 007HF rotating anode generator with Varimax™ optics.

For synchrotron data collection, the SSRL Automated Mounting system (SAM) was used. Mounted crystals were flash-frozen in liquid nitrogen and placed in the SAM cassettes. Diffraction data were collected at the Australian Synchrotron, Beamline MX1 using X-rays of wavelength 0.95 Å.

Data processing, structural solution and refinement. Crystal data sets were integrated, merged and scaled with either HKL2000[46] or MOSFLM and SCALA of the CCP4 software package.[47] The structures were solved by molecular replacement with CCP4 using the Protein Data Bank entry 1MMI as a starting model. Iterative model building and refinement was done with Refmac5[48] and Coot[49].

Fluorescence polarization assay. All FP experiments were conducted with a POLARstar Omega plate reader using non-treated black sterile 96-well plates (Greiner, USA). The buffer contains 10 mM HEPES (pH 7.4), 1mM EDTA, 1 mM DTT, 0.07% Nonidet P-40 and 5% DMSO. Various fluorescently-labeled peptides were designed and tested. One fluorescent peptide, 5'-Fluorescein(FAM)-QLDLF-OH (GL Biochem, China) with >95% purity confirmed

by HPLC-MS, was used for the competition assay with 10 nM of tracer and 50 nM of the SC monomer. Blank control (buffer), negative control (buffer and the peptide) and positive control (buffer, peptide and the SC) were used for data standardization to yield the extent of inhibition. Experiments were carried out in duplicate. Curves were fitted using GraphPad Prism v5.01 (GraphPad Software, USA). Binding-saturation curve fitting was applied to tracer binding. Dose-response curve fitting was applied to competition assays with variable slope, constraining Top at 100 and Bottom at 0.

Isothermal Titration Calorimetry. ITC was performed using a MicroCal Auto-iTC200 calorimeter (Microcal, GE Healthcare) at 298 K. The SC was dialyzed against a buffer (10 mM HEPES pH 7.2, 0.15 M NaCl and 1 mM EDTA) and the same buffer was used to dissolve the peptides. The feedback mode was "high" with the reference power setting of 10 $\mu cals^{-1}$. The cell was stirred at 1000 rpm and the thermostat at 25 °C. Experiments were conducted with 19 injections of 2 µL in 4s with 200s spacing. The first injection of 0.4 µl was discarded in all cases. Peptides of 2-5 mM were titrated in sequential injections (2 µl each) into 54 or 90 µM SC monomer. Data were corrected for control experiments with peptide titrated into buffer only. Data analysis was carried out with Origin 7.0 using one-site binding data fitting.

Molecular dynamics simulation, molecular mechanics calculation and Steered molecular dynamics simulation. MD/SMD simulations were carried out with the AMBER 11 software package[39] and the procedures followed the published methods.[37] Details are included in the supporting information.

ASSOCIATED CONTENT

Supporting Information. Crystallographic data, ITC data, tested dipeptides, additional computational data and figures, detailed materials and methods. This material is available free of charge *via* the Internet at http://pubs.acs.org.

Accession Codes. The atomic coordinates and structure factors for $SC^{AcALDLF}$, $SC^{AcQADLF}$, $SC^{AcQLALF}$, $SC^{AcQLDAF}$, $SC^{AcQLDLA}$, SC^{AcLF}, SC^{4MF}, and SC^{P1} have been deposited with the protein data bank under accession codes 4K3M, 4K3O, 4K3P, 4K3Q, 4K3R, 4K3L, 4K3K and 4K3S, respectively.

AUTHOR INFORMATION

Corresponding Author

* aarono@uow.edu.au; phone: +61-42214347

ACKNOWLEDGMENT

We are grateful to Prof. Peter Lewis and Dr. Cong Ma at University of Newcastle for assisting with the ITC experiments. We thank Dr. Haibo Yu for discussion in computational chemistry and the staff at Beamline MX1, Australian Synchrotron. This research was supported by an Australian Research Council (ARC) Discovery Project (DP110100660). Aaron Oakley acknowledges support from the ARC for his Future Fellowship (FT0990287).

ABBREVIATIONS

SC, sliding clamp; LM, linear motif; Ac, acetyl group; PCNA: proliferating cell nuclear antigen; SMD, steered molecular dynamics simulation; ABPA, almost buried polar atoms; FP, fluorescence polarization; MD, molecular dynamics simulation; MM, molecular mechanics; PBSA, Poisson Boltzmann surface area; PDB, protein data bank; SASA, solvent accessible surface area; SPR, surface plasmon resonance; ITC, isothermal titration calorimetry; IC_{50}, half-

maximum inhibitory concentration; SH2, Src homology 2; SH3, Src homology 3; MDM2, Mouse double minute 2 homolog.

REFERENCES

(1) Wilson, A. J. Inhibition of protein-protein interactions using designed molecules. *Chem Soc Rev* **2009,** 38, 3289-3300.

(2) Fong, J. H.; Shoemaker, B. A.; Garbuzynskiy, S. O.; Lobanov, M. Y.; Galzitskaya, O. V.; Panchenko, A. R. Intrinsic disorder in protein interactions: insights from a comprehensive structural analysis. *PLoS Comput Biol* **2009,** 5, e1000316.

(3) Meszaros, B.; Tompa, P.; Simon, I.; Dosztanyi, Z. Molecular principles of the interactions of disordered proteins. *J Mol Biol* **2007,** 372, 549-561.

(4) Gould, C. M.; Diella, F.; Via, A.; Puntervoll, P.; Gemund, C.; Chabanis-Davidson, S.; Michael, S.; Sayadi, A.; Bryne, J. C.; Chica, C.; Seiler, M.; Davey, N. E.; Haslam, N.; Weatheritt, R. J.; Budd, A.; Hughes, T.; Pas, J.; Rychlewski, L.; Trave, G.; Aasland, R.; Helmer-Citterich, M.; Linding, R.; Gibson, T. J. ELM: the status of the 2010 eukaryotic linear motif resource. *Nucleic Acids Res* **2010,** 38, D167-180.

(5) Pawson, T.; Nash, P. Assembly of cell regulatory systems through protein interaction domains. *Science* **2003,** 300, 445-452.

(6) Puntervoll, P.; Linding, R.; Gemund, C.; Chabanis-Davidson, S.; Mattingsdal, M.; Cameron, S.; Martin, D. M.; Ausiello, G.; Brannetti, B.; Costantini, A.; Ferre, F.; Maselli, V.; Via, A.; Cesareni, G.; Diella, F.; Superti-Furga, G.; Wyrwicz, L.; Ramu, C.; McGuigan, C.; Gudavalli, R.; Letunic, I.; Bork, P.; Rychlewski, L.; Kuster, B.; Helmer-Citterich, M.; Hunter, W. N.; Aasland, R.; Gibson, T. J. ELM server: A new resource for investigating short functional sites in modular eukaryotic proteins. *Nucleic Acids Res* **2003,** 31, 3625-3630.

(7) Stein, A.; Pache, R. A.; Bernado, P.; Pons, M.; Aloy, P. Dynamic interactions of proteins in complex networks: a more structured view. *FEBS J* **2009,** 276, 5390-5405.

(8) Nooren, I. M.; Thornton, J. M. Diversity of protein-protein interactions. *EMBO J* **2003,** 22, 3486-3492.

(9) Dyson, H. J.; Wright, P. E. Intrinsically unstructured proteins and their functions. *Nat Rev Mol Cell Biol* **2005,** 6, 197-208.

(10) Humphris, E. L.; Kortemme, T. Design of multi-specificity in protein interfaces. *PLoS Comput Biol* **2007,** 3, e164.

(11) Kim, P. M.; Lu, L. J.; Xia, Y.; Gerstein, M. B. Relating three-dimensional structures to protein networks provides evolutionary insights. *Science* **2006,** 314, 1938-1941.

(12) Shoemaker, B. A.; Portman, J. J.; Wolynes, P. G. Speeding molecular recognition by using the folding funnel: the fly-casting mechanism. *Proc Natl Acad Sci U S A* **2000,** 97, 8868-8873.

(13) Lacy, E. R.; Filippov, I.; Lewis, W. S.; Otieno, S.; Xiao, L.; Weiss, S.; Hengst, L.; Kriwacki, R. W. p27 binds cyclin-CDK complexes through a sequential mechanism involving binding-induced protein folding. *Nat Struct Mol Biol* **2004,** 11, 358-364.

(14) Tang, X.; Orlicky, S.; Mittag, T.; Csizmok, V.; Pawson, T.; Forman-Kay, J. D.; Sicheri, F.; Tyers, M. Composite low affinity interactions dictate recognition of the cyclin-dependent kinase inhibitor Sic1 by the SCFCdc4 ubiquitin ligase. *Proc Natl Acad Sci U S A* **2012,** 109, 3287-3292.

(15) Stein, A.; Aloy, P. Contextual specificity in peptide-mediated protein interactions. *PLoS One* **2008,** 3, e2524.

(16) London, N.; Movshovitz-Attias, D.; Schueler-Furman, O. The structural basis of peptide-protein binding strategies. *Structure* **2010,** 18, 188-199.

(17) Diella, F.; Haslam, N.; Chica, C.; Budd, A.; Michael, S.; Brown, N. P.; Trave, G.; Gibson, T. J. Understanding eukaryotic linear motifs and their role in cell signaling and regulation. *Front Biosci* **2008,** 13, 6580-6603.

(18) Killian, B. J.; Kravitz, J. Y.; Somani, S.; Dasgupta, P.; Pang, Y. P.; Gilson, M. K. Configurational entropy in protein-peptide binding: computational study of Tsg101 ubiquitin E2 variant domain with an HIV-derived PTAP nonapeptide. *J Mol Biol* **2009,** 389, 315-335.

(19) Gunasekaran, K.; Tsai, C. J.; Nussinov, R. Analysis of ordered and disordered protein complexes reveals structural features discriminating between stable and unstable monomers. *J Mol Biol* **2004,** 341, 1327-1341.

(20) Fuxreiter, M.; Tompa, P.; Simon, I. Local structural disorder imparts plasticity on linear motifs. *Bioinformatics* **2007,** 23, 950-956.

(21) Csizmok, V.; Bokor, M.; Banki, P.; Klement, E.; Medzihradszky, K. F.; Friedrich, P.; Tompa, K.; Tompa, P. Primary contact sites in intrinsically unstructured proteins: the case of calpastatin and microtubule-associated protein 2. *Biochemistry* **2005,** 44, 3955-3964.

(22) Vassilev, L. T.; Vu, B. T.; Graves, B.; Carvajal, D.; Podlaski, F.; Filipovic, Z.; Kong, N.; Kammlott, U.; Lukacs, C.; Klein, C.; Fotouhi, N.; Liu, E. A. In vivo activation of the p53 pathway by small-molecule antagonists of MDM2. *Science* **2004,** 303, 844-848.

(23) Rudolph, J. Inhibiting transient protein-protein interactions: lessons from the Cdc25 protein tyrosine phosphatases. *Nat Rev Cancer* **2007,** 7, 202-211.

(24) Lopez de Saro, F. J.; Georgescu, R. E.; Goodman, M. F.; O'Donnell, M. Competitive processivity-clamp usage by DNA polymerases during DNA replication and repair. *EMBO J* **2003,** 22, 6408-6418.

(25) Indiani, C.; O'Donnell, M. The replication clamp-loading machine at work in the three domains of life. *Nat Rev Mol Cell Biol* **2006,** 7, 751-761.

(26) Kong, X. P.; Onrust, R.; O'Donnell, M.; Kuriyan, J. Three-dimensional structure of the beta subunit of E. coli DNA polymerase III holoenzyme: a sliding DNA clamp. *Cell* **1992,** 69, 425-437.

(27) Shamoo, Y.; Steitz, T. A. Building a replisome from interacting pieces: sliding clamp complexed to a peptide from DNA polymerase and a polymerase editing complex. *Cell* **1999,** 99, 155-166.

(28) Lopez de Saro, F. J. Regulation of interactions with sliding clamps during DNA replication and repair. *Curr Genomics* **2009,** 10, 206-215.

(29) Lopez de Saro, F. J.; O'Donnell, M. Interaction of the beta sliding clamp with MutS, ligase, and DNA polymerase I. *Proc Natl Acad Sci U S A* **2001,** 98, 8376-8380.

(30) Robinson, A.; Causer, R. J.; Dixon, N. E. Architecture and conservation of the bacterial DNA replication machinery, an underexploited drug target. *Curr Drug Targets* **2012,** 13, 352-372.

(31) Wijffels, G.; Johnson, W. M.; Oakley, A. J.; Turner, K.; Epa, V. C.; Briscoe, S. J.; Polley, M.; Liepa, A. J.; Hofmann, A.; Buchardt, J.; Christensen, C.; Prosselkov, P.; Dalrymple, B. P.; Alewood, P. F.; Jennings, P. A.; Dixon, N. E.; Winkler, D. A. Binding inhibitors of the bacterial sliding clamp by design. *J Med Chem* **2011,** 54, 4831-4838.

(32) Wijffels, G.; Dalrymple, B. P.; Prosselkov, P.; Kongsuwan, K.; Epa, V. C.; Lilley, P. E.; Jergic, S.; Buchardt, J.; Brown, S. E.; Alewood, P. F.; Jennings, P. A.; Dixon, N. E. Inhibition of protein interactions with the beta 2 sliding clamp of Escherichia coli DNA polymerase III by peptides from beta 2-binding proteins. *Biochemistry* **2004,** 43, 5661-5671.

(33) Kongsuwan, K.; Josh, P.; Picault, M. J.; Wijffels, G.; Dalrymple, B. The plasmid RK2 replication initiator protein (TrfA) binds to the sliding clamp beta subunit of DNA polymerase III: implication for the toxicity of a peptide derived from the amino-terminal portion of 33-kilodalton TrfA. *J Bacteriol* **2006,** 188, 5501-5509.

(34) Burnouf, D. Y.; Olieric, V.; Wagner, J.; Fujii, S.; Reinbolt, J.; Fuchs, R. P.; Dumas, P. Structural and biochemical analysis of sliding clamp/ligand interactions suggest a competition between replicative and translesion DNA polymerases. *J Mol Biol* **2004,** 335, 1187-1197.

(35) Georgescu, R. E.; Yurieva, O.; Kim, S. S.; Kuriyan, J.; Kong, X. P.; O'Donnell, M. Structure of a small-molecule inhibitor of a DNA polymerase sliding clamp. *Proc Natl Acad Sci U S A* **2008,** 105, 11116-11121.

(36) Wolff, P.; Olieric, V.; Briand, J. P.; Chaloin, O.; Dejaegere, A.; Dumas, P.; Ennifar, E.; Guichard, G.; Wagner, J.; Burnouf, D. Y. Structure-based design of short peptide ligands binding onto the E. coli processivity ring. *J Med Chem* **2011,** 54, 4627-4637.

(37) Schmidtke, P.; Luque, F. J.; Murray, J. B.; Barril, X. Shielded hydrogen bonds as structural determinants of binding kinetics: application in drug design. *J Am Chem Soc* **2011,** 133, 18903-18910.

(38) Kenakin, T. *Pharmacologic analysis of drug-receptor interaction*. second edition ed.; Raven Press: 1993.

(39) Case, D. A.; Darden, T. A.; Cheatham, I., T.E. ; Simmerling, C. L.; J. Wang; R.E. Duke; R. Luo; R.C. Walker; W. Zhang; K.M. Merz; B. Roberts; B. Wang; S. Hayik; A. Roitberg; G. Seabra; I. Kolossváry; K.F. Wong; F. Paesani; J. Vanicek; J. Liu; X. Wu; S.R. Brozell; T. Steinbrecher; H. Gohlke; Q. Cai; X. Ye; J. Wang; M.-J. Hsieh; G. Cui; D.R. Roe; D.H. Mathews;

M.G. Seetin; C. Sagui; V. Babin; T. Luchko; S. Gusarov; A. Kovalenko; Kollman, P. A. *AMBER 11*, 2010.

(40) Pancsa, R.; Fuxreiter, M. Interactions via intrinsically disordered regions: what kind of motifs? *IUBMB Life* **2012,** 64, 513-520.

(41) Ytreberg, F. M. Absolute FKBP binding affinities obtained via nonequilibrium unbinding simulations. *J Chem Phys* **2009,** 130, 164906.

(42) Yaffe, M. B.; Elia, A. E. Phosphoserine/threonine-binding domains. *Curr Opin Cell Biol* **2001,** 13, 131-138.

(43) Moarefi, I.; LaFevre-Bernt, M.; Sicheri, F.; Huse, M.; Lee, C. H.; Kuriyan, J.; Miller, W. T. Activation of the Src-family tyrosine kinase Hck by SH3 domain displacement. *Nature* **1997,** 385, 650-653.

(44) Chen, H. F.; Luo, R. Binding induced folding in p53-MDM2 complex. *J Am Chem Soc* **2007,** 129, 2930-2937.

(45) Oakley, A. J.; Prosselkov, P.; Wijffels, G.; Beck, J. L.; Wilce, M. C.; Dixon, N. E. Flexibility revealed by the 1.85 A crystal structure of the beta sliding-clamp subunit of Escherichia coli DNA polymerase III. *Acta Crystallogr D Biol Crystallogr* **2003,** 59, 1192-1199.

(46) Otwinowski, Z.; Minor, W. Processing of X-ray Diffraction Data Collected in Oscillation Mode. In *Methods in Enzymology*, C.W. Carter, J. R. M. S., Eds., Ed. Academic Press: New York, 1997; Vol. 276.

(47) Winn, M. D.; Ballard, C. C.; Cowtan, K. D.; Dodson, E. J.; Emsley, P.; Evans, P. R.; Keegan, R. M.; Krissinel, E. B.; Leslie, A. G.; McCoy, A.; McNicholas, S. J.; Murshudov, G. N.; Pannu, N. S.; Potterton, E. A.; Powell, H. R.; Read, R. J.; Vagin, A.; Wilson, K. S. Overview of

the CCP4 suite and current developments. *Acta Crystallogr D Biol Crystallogr* **2011,** 67, 235-242.

(48) Skubak, P.; Murshudov, G. N.; Pannu, N. S. Direct incorporation of experimental phase information in model refinement. *Acta Crystallogr D Biol Crystallogr* **2004,** 60, 2196-2201.

(49) Emsley, P.; Cowtan, K. Coot: model-building tools for molecular graphics. *Acta Crystallogr D Biol Crystallogr* **2004,** 60, 2126-2132.

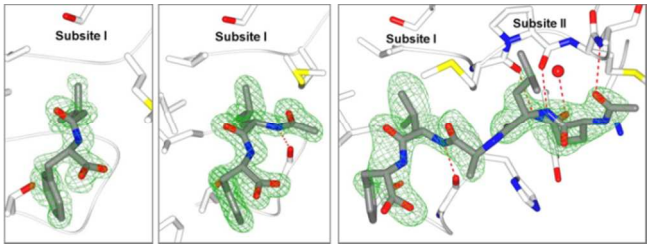

Insert Table of Contents artwork here
